Explosive Leidenfrost droplets

Florian Moreau, Pierre Colinet, Stéphane Dorbolo

Explosive Leidenfrost droplets

Florian Moreau,[1,2,*] Pierre Colinet,[3] and Stéphane Dorbolo[2]

[1] *Institut Pprime, UPR-3346, CNRS, ENSMA, Université de Poitiers, BP 40109, F-86961 Futuroscope Chasseneuil Cedex, France*
[2] *GRASP, Physics Department B5, Université de Liège, B4000-Liège, Belgium*
[3] *Université Libre de Bruxelles, TIPs – Fluid Physics, CP165/67, Avenue F.D. Roosevelt, 50, B-1050 Bruxelles, Belgium*

We show that Leidenfrost droplets made of an aqueous solution of surfactant undergo a violent explosion, for a wide range of initial volumes and concentrations. This unexpected behavior turns out to be triggered by the formation of a gel-like shell during the evaporation when the surface concentration of surfactant reaches some critical value. Shortly later, the temperature sharply increases above the normal boiling point leading to fast bubble growth, shell stretching and explosion. Yet, most of the droplet life is characterized by a self-similar evolution of the radial surfactant distribution during which surface and mean concentrations grow in proportion, independently of the initial conditions. The temperature rise (attributed to boiling point elevation with surface concentration) and nucleation/growth of vapor bubbles inside the shell are key features leading to the explosion, differing from the implosion (buckling) scenario reported by other authors.

I. INTRODUCTION

When a droplet is released over a plate heated above a critical temperature, it levitates above its own vapor. This so-called Leidenfrost effect [1] was discovered a long time ago, yet it remains an active field of research of both fundamental [2–10] and applied [11–13] interests. Recent works have for instance focused on the concave shape of the vapor film underneath the droplet [3–5], on "chimneys" observed above a certain critical size [2, 3], on the abscence of chimneys in particular geometries [14], on take-off regimes observed far below the capillary length [6], and on self-propelled motion on ratchets [15, 16]. In addition to the potential interest of the latter studies for droplet manipulation in microfluidics, understanding the impact of droplets on superheated substrates [7, 8, 13, 17] is crucial for optimizing cooling technologies.

However, most existing studies deal with pure liquids and much less is known about mixtures even though potential applications of the Leidenfrost effect exist (e.g. for nanoparticle deposition [12]). Generally speaking, the evaporation of droplets containing a non-volatile solute (e.g. polymers [18] or colloids [19, 20]) leads to accumulation of the solute near the surface. A gel-like or glassy shell may then form, acquire elastic properties, and buckle (implode) under the internal depression resulting from compression of the shell [18–20].

In this Letter, we show that surfactant molecules (sodium dodecyl sulfate – SDS) in water lead to a quite different Leidenfrost dynamics. Namely, it is reported that after an initial period of gentle evaporation, the life of the droplet quite generally ends up in a sudden explosion, instead of buckling (see an example in Fig. 1a, and the movies $M1$ and $M2$ in the Supplemental Materials [21]).

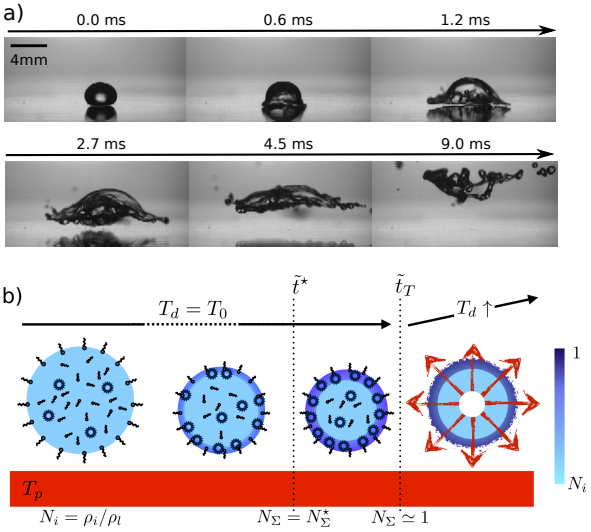

FIG. 1. a. Example of an explosion of a droplet. Initial size of the drop 100 μL, initial concentration 10 CMC and temperature of the plate 400°C. b. Schematic representation of a droplet life. To begin with, free molecules and micelles are uniformly distributed. During the evaporation, the droplet shrinks and micelles accumulate at its surface, leading from $\tilde{t} = \tilde{t}^*$ to the formation of a gel-like shell. From $\tilde{t} = \tilde{t}_T$ the temperature of the droplet, T_d, rises above the boiling temperature T_0, leading to vapor bubble nucleation, growth, shell stretching and finally explosion of the droplet. N denotes the SDS mass fraction and ρ the density (with subscripts i, l and Σ for "initial", "liquid" and "surface", respectively).

Besides a possible impact on applications mentioned above, it is of fundamental interest to understand this unexpected yet reproducible scenario. We here focus on identifying mechanisms leading to explosion, rationalizing experiments made in a wide range of conditions thanks to a simple model based on a spherical symmetry. Formation of a gel-like shell at the droplet surface also turns out to occur with SDS, but the essential new fea-

* florian.moreau@ensma.fr

ture here is a sharp temperature increase of the droplet above the normal boiling point. This is shown to promote rapid growth of vapor bubbles in the water-rich core leading to an overpressure build-up due to the resulting shell stretching, rather than the underpressure-induced shell buckling observed in isothermal conditions [18–20].

II. EXPERIMENTAL SET-UP

Each droplet was placed on a curved and heated plate of aluminum. The curvature allowed to trap the droplet without contact. A heating device, a PID controller and a thermocouple placed at the surface of the plate, were used to control its temperature from $T_p = 200$ to 450°C. A highspeed video camera (IDT-Y4) recorded (up to 30000 fps) a side-view of the droplet evolution during the experiment, enabling extraction of the droplet volume versus time (assuming an axisymmetric shape). The droplet temperature was also followed from the top using an Infra-Red (Flir Thermovision 160) camera. Several concentrations were considered from pure water to 10 times the critical micelle concentration (CMC). Note that for SDS, CMC = 2.37 g/L.

III. RESULTS AND ANALYSIS

A. Volume and concentration evolution

In order to identify the parameters influencing the explosion, the roles of initial concentration and initial volume were analyzed first. Drops of several initial concentrations from pure water to 10 CMC, and several initial sizes from 10 to 1000 μL, were released on the plate heated at 300°C. The corresponding volumes $V(t)$ are plotted versus time t in Fig. 2a. Each curve is the average of 10 experiments. For clarity, curves corresponding to pure water (no explosion) are omitted from this plot.

Fig. 2a shows that for a given starting volume, the initial concentration does not affect the evaporation dynamics. Moreover, it is seen that decreasing the initial volume V_i by some given factor and increasing the initial concentration ρ_i by the same factor, yields nearly the same value of the volume just before explosion V_f. As SDS does not evaporate, one concludes that the mean concentration $\rho_{m,f} = \rho_i V_i / V_f$ at this moment is nearly the same. This suggests that an important parameter to predict the explosion is the mean concentration of surfactant $\rho_m(t) = \rho_i V_i / V(t)$, which is indeed confirmed by plotting ρ_m versus time in Fig. 2b. Whatever the initial size and volume, the mean SDS concentration just before explosion remains in a relatively narrow range of values. Correspondingly, the total mass $m_i = \rho_i V_i$ of SDS inside the droplets depends linearly on the volume before explosion (Fig. 2c), with a slope equal to the value of the critical mean concentration $\rho_{m,f} = 275 \pm 30$ g/L.

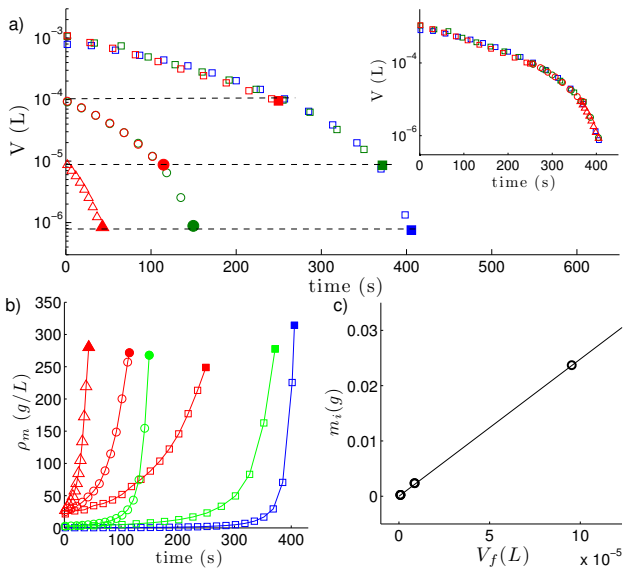

FIG. 2. a. Volume vs time for water/SDS droplets of several initial sizes (V_i) and initial SDS mass concentrations (ρ_i): □ (V_i=1000μL ρ_i=0.1CMC) □ (V_i=1000μL ρ_i=CMC) □ (V_i=1000μL ρ_i=10CMC) ○ (V_i=100μL ρ_i=CMC) ○ (V_i = 100μL ρ_i=10CMC) △ (V_i=10μL ρ_i=10CMC). Filled symbols are used for the final volume just before the explosion. The plate temperature was $T_p = 300$°C. In the inset, a time translation is applied to the data, so as to shift the volume just before explosion onto a reference curve (selected as the one corresponding to $V_i = 1000$ μL $\rho_i = 0.1$ CMC).
b. Mean concentration $\rho_m = \rho_i V_i / V(t)$ versus time. The symbols are the same as in a.
c. Initial mass $m_i = \rho_i V_i$ of SDS vs final volume just before explosion V_f, for all experiments at $T_p = 300$°C. ○: measurement and solid line: interpolation).

An additional observation is that during the droplet life, the evaporation dynamics is largely independent on the initial conditions. This is shown by the inset of Fig. 2a, obtained by horizontally translating curves of the main plot such as to superpose them on a reference curve (here selected as the one spanning the largest range of times and volumes, i.e. for $V_i = 1000$ μL and $\rho_i = 0.1$ CMC). All curves indeed collapse on the reference curve, showing that the drying dynamics is rather independent of the SDS concentration.

This independence with respect to initial conditions and the existence of a critical value of ρ_m may be understood on the basis of scaling analysis. Assuming a small spherical droplet of radius $R(t)$, a "full-surface" conduction-limited evaporation model (see e.g. [2]) yields $\dot{R} \sim -\chi/R$, where $\chi = \lambda_v \theta / \rho_l \mathcal{L}$, in which λ_v is the vapor thermal conductivity, θ the plate superheat (difference between plate temperature T_p and boiling temperature T_0), ρ_l is the liquid density and $\mathcal{L}$ its latent heat. Clearly, evaporation is not affected by SDS, as long as the latter has no effect on liquid properties, and in particular on the boiling temperature. On the other hand, SDS cer-

tainly does not remain uniformly distributed inside the shrinking droplet (Fig. 1b). Assuming the concentration to be above CMC, the non-volatile SDS micelles accumulate within a surface concentration boundary layer of thickness $e(t) \sim D/|\dot{R}| \sim \epsilon R(t)$, where

$$\epsilon = \frac{\rho_l \mathcal{L} D}{\lambda_v \theta} \tag{1}$$

in which D is the diffusion coefficient of micelles. Importantly, note that ϵ therefore measures the boundary layer thickness relative to the droplet radius, and is small provided the superheat θ is sufficiently large. In this case, the volume contained inside this boundary layer at time t is of order $\epsilon V(t)$, and it can be shown by expressing the SDS mass conservation at time t that the concentration ρ_Σ at the surface (i.e. in the boundary layer) scales as

$$\rho_\Sigma(t) - \rho_i \sim \frac{\rho_i \left[V_i - V(t)\right]}{\epsilon V(t)} = \frac{\rho_m(t) - \rho_i}{\epsilon} \tag{2}$$

as indeed, $\rho_i(V_i - V)$ is the mass of surfactant which has accumulated inside the boundary layer, at time t, as a result of droplet shrinkage from V_i to V. Note also that outside the boundary layer, we assume the concentration remains equal to ρ_i. Hence, if $\rho_m \gg \rho_i$ (always valid before explosion for our conditions, see Fig. 2), Eq. (2) yields $\rho_\Sigma \sim \rho_m/\epsilon$, i.e. a *direct link* between the mean concentration ρ_m and the surface concentration ρ_Σ, independent of V_i and ρ_i. Thus, the critical value of ρ_m evidenced above corresponds to a critical value of ρ_Σ, which actually makes more sense physically. On this basis, our working assumption in what follows is that the explosion sequence starts when the surface concentration reaches a well-defined critical value ρ^*_Σ . Hereafter, this conjecture will be reinforced by the direct observation of the formation of a gel-like shell at the droplet surface, and by pushing our modeling further.

Coming back to experiments, the influence of the superheat θ was then considered. Drops were released on the plate at several temperatures from 200 to 450°C. The drops had the same initial size $V_i = 100$ μL, and the same initial SDS concentration $\rho_i = 10$ CMC. The evolution of the volume is plotted in Fig. 3a. Each curve is the average of 5 experiments. Expectedly, a higher plate temperature results in a shorter evaporation time. The values of the volume just before the explosion are plotted in Fig. 3b. They all lie in the range 9.8±1.2 μL, but increasing the plate temperature clearly results in a higher volume before the explosion. This tendency is actually coherent with the above scaling analysis, which predicts a final volume $V_f \sim \rho_i V_i/\epsilon\rho^*_\Sigma$, indeed increasing with θ (but faster than in Fig. 3b, likely due to the simplicity of our model and to the fact that ρ^*_Σ itself may slightly increase with the evaporation rate). Note finally that below 250°C no explosion occurs (see also [22]). In this case, at the end of the droplet life, a residue made of non-evaporated products gently comes in contact with the hot surface without explosion.

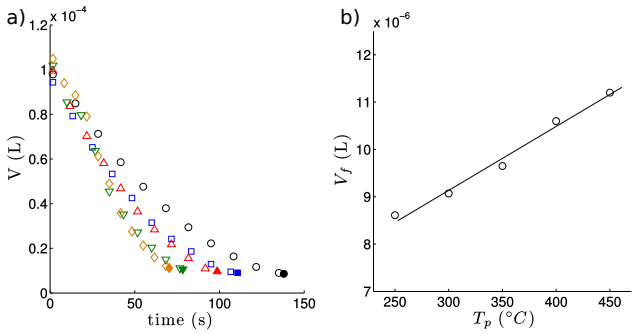

FIG. 3. a. Volume vs time for water/SDS droplets at several temperatures of the plate: ◯ 250°C □ 300°C △ 350°C ▽ 400°C ◇ 450°C. Filled symbols are used for the final volume before the explosion. The initial concentration of the droplet is 10 CMC and the initial size of the droplet is 100 μL.
b. The final volume before explosion, V_f is plotted vs the temperature of the plate T_p. The line is a linear fit.

B. Shell formation and temperature increase

Careful analysis of high-speed movies revealed that, at a certain time before the explosion, a shell is formed around the droplet. Just before the explosion, a capillary tube was used to remove the droplet (still in Leidenfrost state) from the hot plate to bring it on a plate at room temperature (see Fig. 4a). The liquid turns out to be encapsulated within a gel-like shell covering the whole droplet. This observation clearly demonstrates that the presence of the shell does not prevent the droplet to be in Leidenfrost state, at least for some time (typically 10 s).

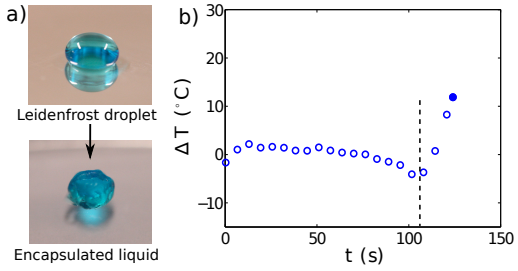

FIG. 4. a. Encapsulation of a Leidenfrost drop. Top: Leidenfrost droplet of SDS, methylene blue and water over a plate at 300°C. Bottom: the Leidenfrost droplet is removed from the hot plate after the shell is formed and put on a cold plate. The whole droplet is covered by the shell, retaining water.
b. Evolution of the temperature of the top part of the droplet surface. The temperature T is measured using an IR camera placed above the droplet (after a calibration procedure), and $\Delta T(t) = T_d(t) - \langle T \rangle_{\text{before shell formation}}$. The dashed line corresponds to the beginning of the formation of the shell.

To understand the nature of this shell, nuclear magnetic resonance spectroscopy was used. Spectrum analysis showed that the shell is made of unaltered SDS molecules. The temperature of the droplet was also mea-

sured from the top using an IR camera, averaging it all over the top surface. A camera simultaneously recorded the droplet shape and the formation of the shell. An example of temperature evolution is shown in Fig. 4b, representing the difference between the temperature at a time t and the time-averaged temperature before shell formation. Even though such IR measurements are generally delicate in the case of droplets, a sudden increase of temperature (possibly preceded by a slight decrease) is clearly detected after the shell formation. This increase generally exceeds 10°C, and can therefore be expected to be a precursor of the explosion (given moreover that even higher temperatures are expected under the drop).

C. Self-similar concentration profile evolution

To gain further insight into this complex process, the evolution of the SDS mass fraction profile $N(r,t) = \rho(r,t)/\rho_l$ is now analyzed in more details, yet still assuming a spherical droplet of radius $R(t)$ in its vapor at temperature T_p. As for the droplet temperature T_d, the sharp increase observed in Fig. 4b can be modeled by assuming that it follows the equilibrium curve $T_{\rm eq}(N_\Sigma)$, depending on the surface mass fraction $N_\Sigma = N|_{r=R}$. This is indeed the natural generalization of the usual condition for pure liquids, namely $T_d = T_0 = T_{\rm eq}(0)$ (normal boiling point). However, to our knowledge the curve $T_{\rm eq}(N)$ is unknown and delicate to measure at large N. As our own experiments did not detect any such boiling point elevation up to $N = 0.35$, and since thermodynamics of ideal solutions shows that $T_{\rm eq}$ does not deviate from $T_0 = 373$K before N gets very close to unity (due to the large molar weight of SDS micelles), we here stick to $T_d = T_0$. Then, rescaling distances by the initial radius R_i and time by the evaporation time $\tau_e = \rho_l \mathcal{L} R_i^2/2\lambda_v\theta$ of a SDS-free droplet, the dimensionless radius evolves according to $\partial_{\tilde t}\tilde R = -(2\tilde R)^{-1}$ as before, while $N(\tilde r,\tilde t)$ satisfies the diffusion equation $2\,\partial_{\tilde t} N = \epsilon\,\tilde r^{-2}\partial_{\tilde r}(\tilde r^2\partial_{\tilde r}N)$ with boundary conditions $\partial_{\tilde r}N|_{\tilde r=0} = 0$ (symmetry) and $\epsilon\tilde R\,N^{-1}\partial_{\tilde r}N|_{\tilde r=\tilde R} = 1$ (no SDS flux through the surface). Note that ϵ, as defined by Eq. (1), is the natural dimensionless parameter characterizing this Stefan-like problem. Integrating the equation for $\tilde R$ directly yields $\tilde R = (1-\tilde t)^{1/2}$, and from the total SDS mass conservation we readily obtain the mean mass fraction $N_m = N_i/\tilde R^3$. This suggests a self-similar solution for N, namely

$$N(\tilde r,\tilde t) = \frac{N_i}{\tilde R^3} F_0(\epsilon)\exp\left[\frac{\tilde r^2}{2\epsilon\tilde R^2}\right] \qquad (3)$$

which indeed solves the above-stated problem, and where

$$F_0(\epsilon) = 3^{-1}\left(\epsilon\exp[1/2\epsilon] - \sqrt{\pi/2}\,\epsilon^{3/2}\mathrm{erfi}\left[1/\sqrt{2\epsilon}\right]\right)^{-1}$$

is a normalisation factor found from the definition of $N_m = 3\tilde R^{-3}\int_0^{\tilde R}\tilde r^2 N(\tilde r,\tilde t)d\tilde r$ (solute mass conservation) and $\mathrm{erfi}[z]$ is the imaginary error function $\mathrm{erf}[iz]/i$.

The similarity solution (3) is actually valid after a short transient, when the actual initial condition has been forgotten. In this regime, rescaling N by N_m and r by R collapses all concentration profiles onto a single curve, independently of the initial volume and concentration. Moreover, Eq. (3) shows that the ratio $N_\Sigma/N_m = F_0(\epsilon)\exp[1/2\epsilon] = F_1(\epsilon)$ is a constant, i.e. surface and mean values of N grow in proportion during the droplet evaporation. This not only confirms Eq. (2) for $N_i \ll 1$ but generalizes it to $O(1)$ values of ϵ, and enables estimating the value $N_\Sigma^* = \rho_\Sigma^*/\rho_l$ at which a shell forms at the free surface, as conjectured above. Namely, using experimental values of N_m at shell formation for various values of the plate temperature T_p (and $N_i = 0.024$, i.e. $\rho_i = 10$ CMC), we obtain values of N_Σ^* between 0.37 and 0.69, i.e. a range where phase transitions of the SDS solution are indeed expected [23]. Note that for estimating ϵ, we used Stokes-Einstein law $D = kT/6\pi\eta r_0$ with $r_0 = 17$Å , the radius of a SDS micelle, and λ_v was evaluated at $(T_p+T_0)/2$. Remark finally that N_Σ^* is found to increase with the plate temperature (hence with the evaporation rate), which might be due to faster quenching and delayed nucleation of the gel-like phase. As already mentioned, this could also be linked to the simplicity of our spherically-symmetric model, which "averages out" any non-homogeneity of concentration at the drop surface (we indeed experimentally observe that the growth of the shell is inhomogeneous).

Now, a closer look at Fig. 2b interestingly reveals that the time scale of the concentration increase gets shorter at smaller values of N_i, which is also captured by the self-similar solution Eq. (3). Namely, the time $\tilde t^*$ at which the shell starts to form is readily obtained from the condition $N_\Sigma = N_m F_1(\epsilon) = N_\Sigma^*$ (taken equal to 0.5 hereafter). Using $\tilde R = (1-\tilde t)^{1/2}$, this leads to $\tilde t^* = 1 - [2N_iF_1(\epsilon)]^{2/3}$, showing that shell formation occurs closer to the evaporation time of a pure droplet (of the same initial volume and for the same superheat) when N_i gets smaller. This actually also holds for the time $\tilde t_T > \tilde t^*$ at which the temperature starts to increase, which as said above, corresponds to the moment where $N_\Sigma \simeq 1$. Assuming the fluid properties (and in particular the diffusion coefficient D) to keep the same values in the shell, we similarly get $\tilde t_T = 1-[N_iF_1(\epsilon)]^{2/3}$. Hence, $\tilde t_T - \tilde t^* \sim [N_iF_1(\epsilon)]^{2/3}$, which clearly shows the acceleration of events occurring when N_i decreases. Note that this is also coherent with our experimental observation of more violent explosions for less loaded droplets (see movie M3 in Supplemental Material [21]).

D. Vapor bubble nucleation/growth within shell

At time $\tilde t_T$, the droplet temperature $T_d = T_{\rm eq}(N_\Sigma)$ sharply increases and can get extremely high given that SDS is non-volatile. In theory, T_d can rise up to the plate temperature T_p when the surface mass fraction N_Σ

gets very close to unity (quasi-pure SDS), and the droplet comes in contact with the substrate (the evaporation rate vanishing as $T_p - T_d \to 0$). However, before this ultimate stage is possibly reached, conditions for nucleation of tiny vapor bubble(s) can be met inside the shell, which still contains a lot of water with a boiling temperature close to $T_0 = 373$ K. This water-rich core is therefore in a metastable state as soon as $T_d > T_0$, and homogeneous nucleation will certainly occur for $T_d > T_k = 575$ K [24]. Given moreover that heterogeneous nucleation may occur earlier than that (due to impurities or even micelles themselves), and that the threshold for explosion was found between $T_p = 200°\text{C} = 473$ K and $T_p = 250°\text{C} = 523$ K (see above), a boiling-mediated explosion scenario turns out to be very likely, as now studied in more details.

Consider a spherical droplet of initial radius R_0 at temperature $T_d = T_n$, i.e. assuming that it has already heated up to the nucleation limit T_n (be it homogeneous or heterogeneous). Once nucleated, any bubble grows extremely fast given the large value of the superheat $\Delta T = T_n - T_0 \simeq 200$ K, and of the corresponding Jacob number $\text{Ja} = \rho_l c_{p,l} \Delta T / \rho_v \mathcal{L} \simeq 600$, where $c_{p,l}$ is the liquid heat capacity and ρ_v the vapor density. In these conditions, the time scale of bubble growth up to a size R_0 is of the order of $\tau_b \sim \text{Ja}^{-2} R_0^2/\kappa_l$ (where κ_l is the liquid thermal diffusivity) [25], i.e. very short indeed (about 0.1μs for a 100 μL droplet). Bubble growth up to a size comparable to the containing droplet thus occurs instantaneously on the time scale $\tau_e \sim 10^2$ s of droplet evaporation, and even on the time scale $\tau_i \sim \tau_e N_i^{2/3} \sim 10^0$ s of the concentration/temperature increase.

Now, the droplet is confined by a SDS-rich shell which can be assumed to possess elastic properties, even though the Young's modulus of the various phases of SDS [23] has not been measured, to the best of our knowledge. Clearly, bubble growth within the liquid stretches the shell to a certain extent which may or may not be sufficient for the shell to rupture, i.e. for explosion to occur. Indeed, two effects can limit bubble growth and lead the system to a steady state: i) the finite amount of heat available in the droplet at the moment a bubble nucleates; ii) the rise of internal pressure (induced by the shell stretching) which leads to an increase of the boiling temperature. For each of these effects separately, we may estimate the final stretching ratio $\delta = R_s/R_0 - 1$, where R_s is the droplet radius at steady state. For the effect i), denoting by T_s the final temperature and noting that $\rho_v \ll \rho_l$, the radius b_s (or rather the volume $4\pi b_s^3/3$) of the bubble at steady state can be obtained by dividing the excess heat in the liquid by the latent heat per unit volume of vapor. This simply yields $b_s = R_0 \text{Ja}_\text{s}^{1/3}$, where $\text{Ja}_\text{s} = \rho_l c_{p,l}(T_n - T_s)/\rho_v \mathcal{L}$ is a Jacob number based on the temperature drop $T_n - T_s$. Expressing the conservation of mass then yields a first expression of the stretching ratio for thermally-limited growth:

$$\delta_i = (1 + \text{Ja}_\text{s})^{1/3} - 1 \qquad (4)$$

On the other hand, for case ii), a steady state is reached when the final temperature T_s equals the boiling temperature at pressure $p_0 + \Delta p_i$, where $\Delta p_i = 4E(e_0/R_0)\delta$ is the (linearized) elasticity-induced excess pressure, (as for a balloon) E is the Young's modulus and e_0 is the shell thickness. Using the Clausius-Clapeyron equation and solving for δ, this yields the stretching ratio for stiffness-limited growth:

$$\delta_{ii} = \frac{p_0}{4E}\frac{R_0}{e_0}\left[\exp\left[-\frac{\mathcal{L}M_w}{R_g}\left(\frac{1}{T_s} - \frac{1}{T_0}\right)\right] - 1\right] \qquad (5)$$

where M_w is the molar mass of water and R_g is the perfect gas constant. In general, the solution lies between these two extremes, and can be found by solving $\delta_i = \delta_{ii}$ for T_s. A single solution is found in the interval $[T_0, T_n]$, the limits of which corresponding to thermally-limited growth ($T_s \to T_0$ for small values of the dimensionless stiffness $\sigma = 4Ee_0/R_0p_0$) and stiffness-limited growth ($T_s \to T_n$ for large values of σ). The corresponding stretching ratio is represented in Fig. 5 as a function of the plate temperature T_p (which affects $e_0/R_0 \sim \epsilon$, see above), for a wide range of values of E.

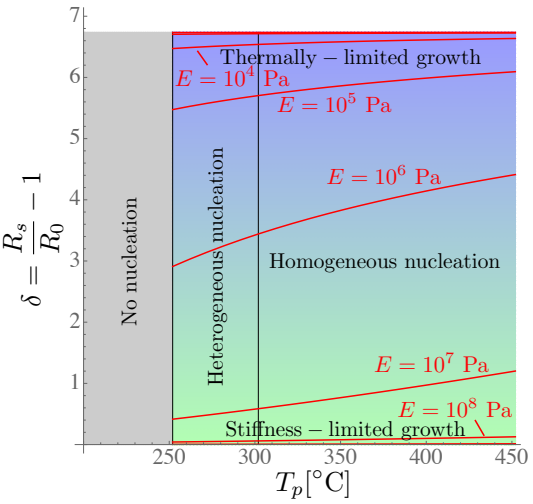

FIG. 5. The stretching ratio $\delta = R_s/R_0 - 1$ of the shell as a function of the plate temperature T_p, for various values of the Young's modulus E. The ratio of shell thickness e_0 to droplet radius R_0 is taken equal to ϵ, which decreases with T_p, leading to a slight increase of δ. Here, $p_0 = 1$ atm, $T_0 = 373$K, and the nucleation temperature is taken (for illustration) to be $T_n = 525$K, i.e. 50K lower than the homogeneous nucleation limit T_k. The zone between $E = 10^3$ Pa and 10^5 Pa corresponds to hydrogels, thought to be representative of our SDS shells. Note that this diagram is independent of the values of V_i and N_i, due to the self-similarity of the concentration evolution discussed above.

Assuming E to be of the order of $10^3 - 10^5$ Pa, as for an hydrogel (given that the SDS skin contains a significant amount of water), it is seen that the shell may be considerably stretched ($\delta \sim 600\%$ is close to its maximal value obtained from Eq. (4) in the thermally-limited case) and therefore highly likely to rupture (hydrogels

can barely withstand about 50% of strain, see e.g. [26]). In fact, it turns out that only very stiff material with moduli above 10^8 Pa could resist internal bubble growth (yet the encapsulated object would contain voids, resembling cavitation bubbles observed in isothermal situations [27]). Therefore, even though accurate measurements of E and δ would certainly be valuable, we believe that the above discussion strongly supports the proposed boiling-induced explosion scenario of Leidenfrost droplets (while thermal expansion alone cannot lead to a significant stretching of the shell).

IV. CONCLUSION

To conclude, we emphasize that the proposed scenario does not require the droplet to contact the plate (see movie $M4$ in the Supplemental Materials [21], in which a vertical jet can be seen below the droplet, followed by the explosion and eventually foam formation). It thus essentially differs from contact boiling [8], in that it relies on the concentration contrast between surface and bulk, the latter becoming prone to nucleate and grow vapor bubbles. We also pointed out an interesting cascade of time scales (successively: droplet evaporation, concentration/temperature increase, and vapor bubble growth), each one essentially shorter than the previous one. Finally, among the many possible perspectives of this work, other types of solutes certainly need to be tested, such as polymers, or colloidal particles, for which the detailed mechanisms might considerably differ. The effect of internal flows generated by the vapor shear [28] is also worth considering, in view of the strong effect it might have on the surfactant concentration profile. Yet, the formation of a shell and the explosion scenario proposed here should not be invalidated, given that flows are expected to remain locally tangential to the drop surface, in addition to being strongly reduced well before shell formation due to the Plateau-Marangoni-Gibbs effect.

ACKNOWLEDGMENTS

The authors gratefully thank C. Sun, S. Lyu, D. Quéré, A. Bouillant, B. Roman and B. Sobac for interesting discussions. This work was supported by the ODILE project (FRFC Contract No. 2.4623.11), and partly by the μ-MAST project (BELSPO IAP 7/38). SD and PC also gratefully acknowledge support of the F.R.S. – FNRS.

[1] J. G. Leidenfrost, *De Aquae Communis Nonnullis Qualitatibus Tractatus* (1756).
[2] A. L. Biance, C. Clanet, and D. Quéré, "Leidenfrost drops," Physics of Fluids **15**, 1632–1637 (2003).
[3] J. H. Snoeijer, P. Brunet, and J. Eggers, "Maximum size of drops levitated by an air cushion," Physical Review E **79**, 036307 (2009).
[4] J. C. Burton, A. L. Sharpe, R. C. A. van der Veen, A. Franco, and S. R. Nagel, "Geometry of the vapor layer under a leidenfrost drop," Phys. Rev. Lett. **109**, 074301– (2012).
[5] B. Sobac, A. Rednikov, S. Dorbolo, and P. Colinet, "Leidenfrost effect: Accurate drop shape modeling and refined scaling laws," Phys. Rev. E **90** (2014).
[6] Franck Celestini, Thomas Frisch, and Yves Pomeau, "Take off of small leidenfrost droplets," Phys. Rev. Lett. **109**, 034501– (2012).
[7] A. L. Biance, C. Pirat, and C. Ybert, "Drop fragmentation due to hole formation during leidenfrost impact," Physics of Fluids **23**, 022104 (2011).
[8] T. Tran, H.J.J. Staat, A. Prosperetti, C. Sun, and D. Lohse, "Drop impact on superheated surfaces," Physical Review Letters **108**, – (2012).
[9] X. Ma, J.-J. Liétor-Santos, and J. C. Burton, "Star-shaped oscillations of leidenfrost drops," Physical Review Fluids **2** (2017).
[10] A. Gauthier, J. C. Bird, C. Clanet, and D. Quéré, "Aerodynamic leidenfrost effect," Physical Review Fluids **1** (2016).
[11] H. Kim, B. Truong, J. Buongiorno, and L. W. Hu, "On the effect of surface roughness height, wettability, and nanoporosity on leidenfrost phenomena," Applied Physics Letters **98**, 083121 (2011).
[12] M. Elbahri, D. Paretkar, K. Hirmas, S. Jebril, and R. Adelung, "Anti-lotus effect for nanostructuring at the leidenfrost temperature," Advanced Materials **19**, 1262–1266 (2007).
[13] A. Labergue, J.-D. Pena-Carillo, M. Gradeck, and F. Lemoine, "Combined three-color lif-pda measurements and infrared thermography applied to the study of the spray impingement on a heated surface above the leidenfrost regime," International Journal of Heat and Mass Transfer **104**, 1008–1021 (2017).
[14] S. Hidalgo-Caballero, Y. Escobar-Ortega, and F. Pacheco-Vazquez, "Leidenfrost phenomenon on conical surfaces," Phys. Rev. Fluids **1**, 051902 (2016).
[15] H. Linke, B. J. Alemán, L. D. Melling, M. J. Taormina, M. J. Francis, C. C. Dow-Hygelund, V. Narayanan, R. P. Taylor, and A. Stout, "Self-propelled leidenfrost droplets," Phys. Rev. Lett. **96**, 154502– (2006).
[16] A. Hashmi, Y. Xu, B. Coder, P.A. Osborne, J. Spafford, G.E. Michael, G. Yu, and J. Xu, "Leidenfrost levitation: Beyond droplets," Scientific Reports **2**, – (2012).
[17] M. A. J. Van Limbeek, P. B. J. Hoefnagels, M. Shirota, C. Sun, and D. Lohse, "Boiling regimes of impacting drops on a heated substrate under reduced pressure," Physical Review Fluids **3** (2018).
[18] L. Pauchard and C. Allain, "Buckling instability induced by polymer solution drying," Europhys. Lett. **62**, 897–903 (2003).
[19] L. Pauchard and Y. Couder, "Invagination during the collapse of an inhomogeneous spheroidal shell," Europhysics Letters **66**, 667–673 (2004).

[20] N. Tsapis, E. R. Dufresne, S. S. Sinha, C. S. Riera, J. W. Hutchinson, L. Mahadevan, and D. A. Weitz, "Onset of buckling in drying droplets of colloidal suspensions," Phys. Rev. Lett. **94**, 018302– (2005).

[21] See Supplemental Material at [URL will be inserted by publisher] for supplementary movies. The movies show several explosions under several conditions. The description of the videos can be found in the README.txt file.

[22] Y.M. Qiao and S. Chandra, "Experiments on adding a surfactant to water drops boiling on a hot surface," Proceedings of the Royal Society A: Mathematical, Physical and Engineering Sciences **453**, 673–689 (1997).

[23] P Kekicheff, C Grabielle-Madelmont, and M Ollivon, "Phase diagram of sodium dodecyl sulfate-water system: 1. a calorimetric study," Journal of Colloid and Interface Science **131**, 112–132 (1989).

[24] C.T. Avedisian, "The homogeneous nucleation limits of liquids," J. Phys. Chem. Ref. Data **14**, 695–729– (1985).

[25] A. Prosperetti, "Vapor bubbles," Ann. Rev. Fluid Mech. **49**, 221–248– (2017).

[26] G.L. Puleo, F. Zulli, M. Piovanelli, M. Giordano, B. Mazzolai, L. Beccai, and L. Andreozzi, "Mechanical and rheological behavior of pnipaam crosslinked macrohydrogel," Reactive and Functional Polymers **73**, 1306–1318 (2013).

[27] F. Meng, M. Doi, and Z. Ouyang, "Cavitation in drying droplets of soft matter solutions," Phys. Rev. Lett. **113**, 098301 (2014).

[28] A. Bouillant, T. Mouterde, Ph. Bourrianne, A. Lagarde, C. Clanet, and D. Quéré, "Leidenfrost wheels," Nature Physics (2018).